TRANSMISSION OF 2.43 MEV ELECTRONS THROUGH THICK SILICON TARGETS

By

Jag J. Singh
NASA, Langley Research Center

Presented at

The American Physical Society Meeting
Seattle, Washington
August 31 - September 2, 1967

TABLE OF CONTENTS

TRANSMISSION OF 2.43 MEV ELECTRONS THROUGH THICK SILICON TARGETS

By

Jag J. Singh
NASA, Langley Research Center
Langley Station, Hampton, Virginia

ABSTRACT

The energy and angular distribution of electrons transmitted through silicon targets of various thicknesses have been measured for normally incident electrons of energy 2.43 MeV. The transmitted electron spectra were measured with 5 mm deep Si(Li) detectors. The experimental results have been compared with the calculated values obtained by using the NBS program ETRAN-15. This program includes the effects of secondary electrons and photons besides the effects of ionization energy loss fluctuations. The inclusion of these effects in the theoretical calculations has improved the agreement between the theory and the experiment considerably. The electron diffusion length in silicon at 2.43 MeV has been measured to be (2.50 ± 0.10) mm.

INTRODUCTION

There has been a large discrepancy between[1,2,3] the experimental results and the theoretical calculations of the electron transport problem. Complications arise mainly from the statistical nature of the ionization energy loss and the uncertainty of the effective Coulomb interaction between the incident electrons and the atomic nuclei. In principle, one should be able to solve the transport problem exactly if the screening effects of the atomic electrons and the elastic scattering of the incident electrons are known accurately. However, this approach will involve extremely long and tedious calculations on a computer and, in any case, the exact solution for electron-nuclous elastic scattering cross section has not yet been calculated. Consequently, theoretical

electron transport calculations have been, usually, made with various degrees of simplification. The main purpose of the measurements reported here has been to provide experimental check on the theoretical transport calculations. On the basis of such a comparison, one should be able to write a computer code that is not excessively long and tedious and yet predicts the experimental results with a good degree of accuracy. Once such a program has been finally accepted, it could be used to assess the effectiveness of complex engineering shields without having to make actual measurements.

EXPERIMENTAL PROCEDURE

Figure 1 shows the experimental arrangement used in these measurements. A well-collimated, narrow, electron beam of energy (2430 ± 5) KeV from an electrostatic generator was allowed to fall on a circular silicon target. The silicon target thickness ranged from 10 to 60 percent of the continuous slowing down approximation range of incident electrons in silicon. The transmitted electron spectra were measured with a well-shielded and well-collimated 5 mm thick, 80 mm^2 area, planar, lithium drifted silicon detector. Spectra were measured with and without a 5 mm thick aluminum disc in front of the detector assembly. This technique enabled to allow for the X-ray contribution from the target. The detectors were calibrated using Cs^{137} and Bi^{207} electron sources. Figure 2 shows the conversion electron spectra from these sources.

Figure 3 shows the spectra of mono-energetic electrons scattered from a 100μ gms/cm^2 thick gold foil. Notice the steady increase in the full width at half the maximum height (FWHM) of the scattered electron peaks. This is probably due to the combined effects of the increased energy uncertainty at higher electron energies and poorer resolving power of the detectors for higher energy electrons. Figure 4 shows this effect as a function of energy. Beyond an electron energy of 1500 KeV, the FWHM rises steadily, although slowly, with the electron energy. Figure 5 shows (pulse peak height)/(total area under pulse) as a function of the incident electron energy on the gold foil. The information contained in figures 4 and 5 is needed to introduce the effects of finite resolving power of the detection system on the theoretical energy histograms. Figure 6 shows the manner in which the effect is introduced. As seen in the insert, a gaussian with an appropriate tail is drawn such that the area under the histogram matches that under the pulse. This process is repeated for each energy bin and a final, resultant, curve is drawn to represent the complete histogram as shown here.

THEORETICAL CALCULATIONS

Ten thousand normally incident electrons are allowed to enter the plane parallel slabs which are finite in one dimension and infinite in another dimension. The history of individual electrons is followed in the usual condensed random walk technique developed by Berger[6]. In each condensed step, the multiple scattering by atoms is calculated using Goudsmith-Saunderson theory[5]. The individual scattering cross section used is that due to Mott[6] with screening effects as given by

Moliere[7]. The multiple inelastic scattering effects are sampled from the Landau distribution[8], modified in the manner of Blunk and Leisgang[9]. The secondary electrons - both photoelectrons and those resulting from inelastic collisions with the atoms - are included in the transport calculation. For reasons of the necessary manageability of the calculations, the following specific assumptions are made:

(1) The inelastic scattering probability is calculated using Möller[10] approach which disregards electron binding effects. However, this disregard is not expected to have any significant effect at high electron energies.

(2) The electron-position differences in the energy loss, knock-on electron production and multiple elastic scattering are ignored.

(3) The electrons are not allowed to deflect at the time of energetic bremsstrahlung production nor are they allowed to deflect at the time of fast delta-ray production.

(4) The electron diffraction effects are completely ignored. Only one scattering center is considered at a time.

This program is the basis of ETRAN-15 code of NBS[11] which was used to make the theoretical calculations.

EXPERIMENTAL RESULTS

Figure 7 shows a comparison between the experimental spectra and the theoretical electron energy histograms for a number of target thicknesses. Figure 8 shows a similar comparison after modifying the theoretical energy histograms for the finite resolving power of the detection system. From these comparisons, it is concluded that the experimental spectra are wider than the theoretical spectra and that the

theoretical spectrum peaks slightly higher in energy than does the experimental spectrum. Figure 9 shows a comparison between the experimentally observed angular distribution and the theoretically predicted distribution for two different target thicknesses. The agreement is quite good. Figure 10 shows a comparison of the Bethe function with the experimental and theoretical angular distributions. It appears that the Bethe function is in reasonably good agreement with the experiment and the theory. Figure 11 shows the dependence of average electron deflection[1] on the target thickness. After a target thickness of (2.50 ± 0.10) mm, the incident electron beam does not diffuse out any further. This is in contrast with the earlier hypothesis that the electron beam is isotropically distributed after penetration through thick targets.

CONCLUSIONS

From the above discussions, two major conclusions are drawn: (1) The inclusion of energy straggling effects certainly improves the agreement between the theory and the experiment. In previous reports[1], we have compared the experimental results with the theoretical calculations in the continuous slowing down approximation and with partial inclusion of energy loss straggling effects. The agreement was considerably worse than in the present case. It is hoped that a more accurate incorporation of Landau distribution function and inclusion of the correlation effects ignored here will give better results. (2) The use of a generalization of Foldy-Watson equations[12] in evaluating elastic and inelastic electron

scattering may constitute an improvement. The essential feature of this generalization is a more accurate description of the atomic form factor as it enters small angle scattering cross section. The solution of this electron transport equation utilizing these cross sections may lead to better agreement with the experiment.

REFERENCES

1. Singh, J. J.: Bull. Am. Phys. Soc., 10, 68, 1965. Bull. Am. Phys. Soc., 11, 127, 1966. NASA TN-D-3927 (1967).

2. Rester and Rainwater: NASA CR-334 (1965).

3. Jupiter, Merkel, and Parez: Bull. Am. Phys. Soc., 10, 726, 1965.

4. Berger, Martin J.: Mote Carlo Calculation of the Penetration and Diffusion of Fast Charged Particles. Academic Press, pp. 135-215, 1963.

5. Goudsmit and Saunderson: Phys. Rev., 57, 24, 1940. Phys. Rev., 58, 36, 1940.

6. Mott, N. F.: Proc. Roy. Soc., A124, 475, 1929.

7. Moliere, G.: Z. Naturforsch, 2, 133, 1947.

8. Landau, L.: J. Phys., USSR, 8, 201, 1944.

9. Blunk and Leisgang: Z. Physik, 128, 500, 1950.

10. Moller, C.: Ann. Physik, 14, 531, 1932.

11. Berger and Seltzer: NBS Report #9566, 1967 (to be published as an AEC report).

12. Watson, K. M.: Phys. Rev. 118, 886, 1960.

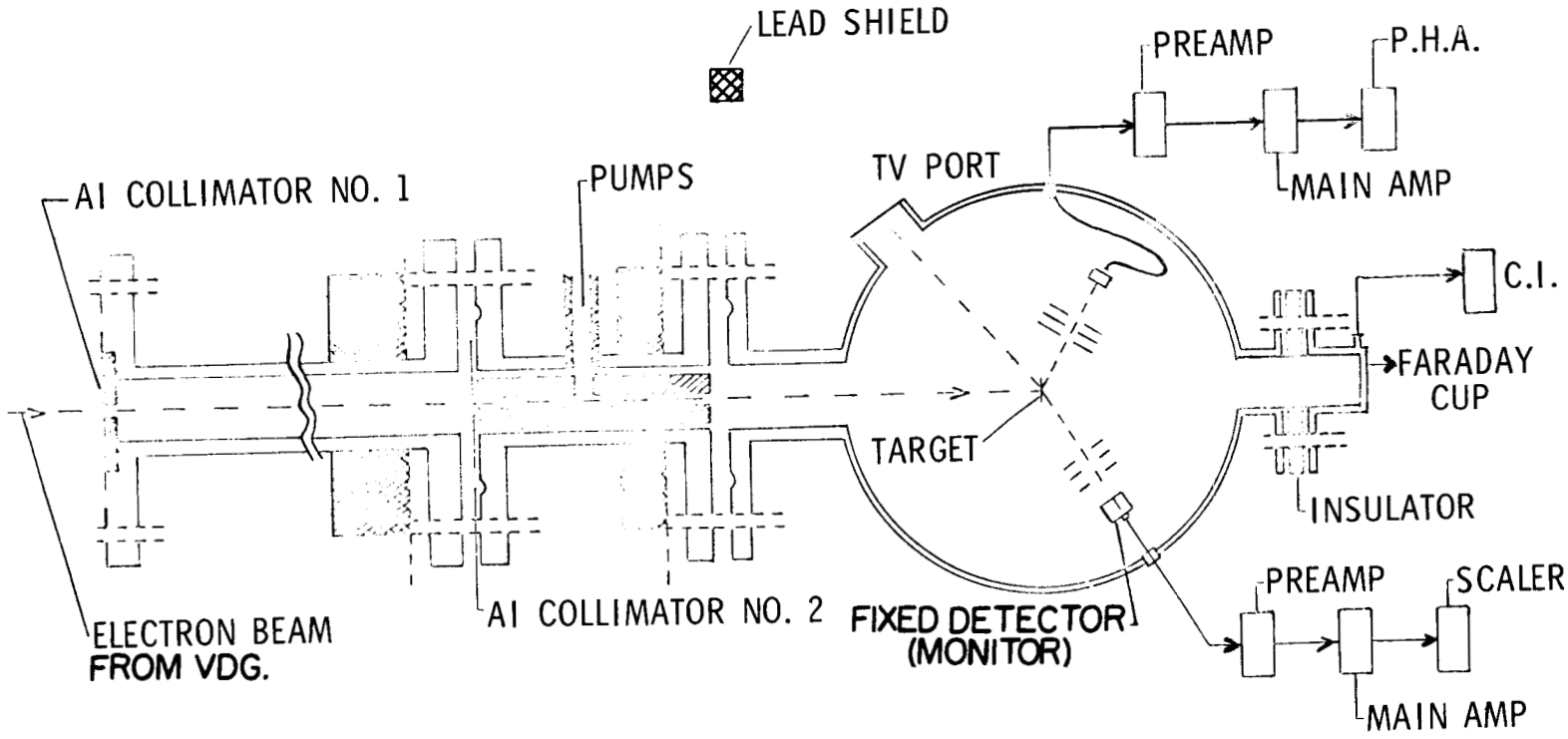

Figure 1.- Schematic diagram of the experimental setup.

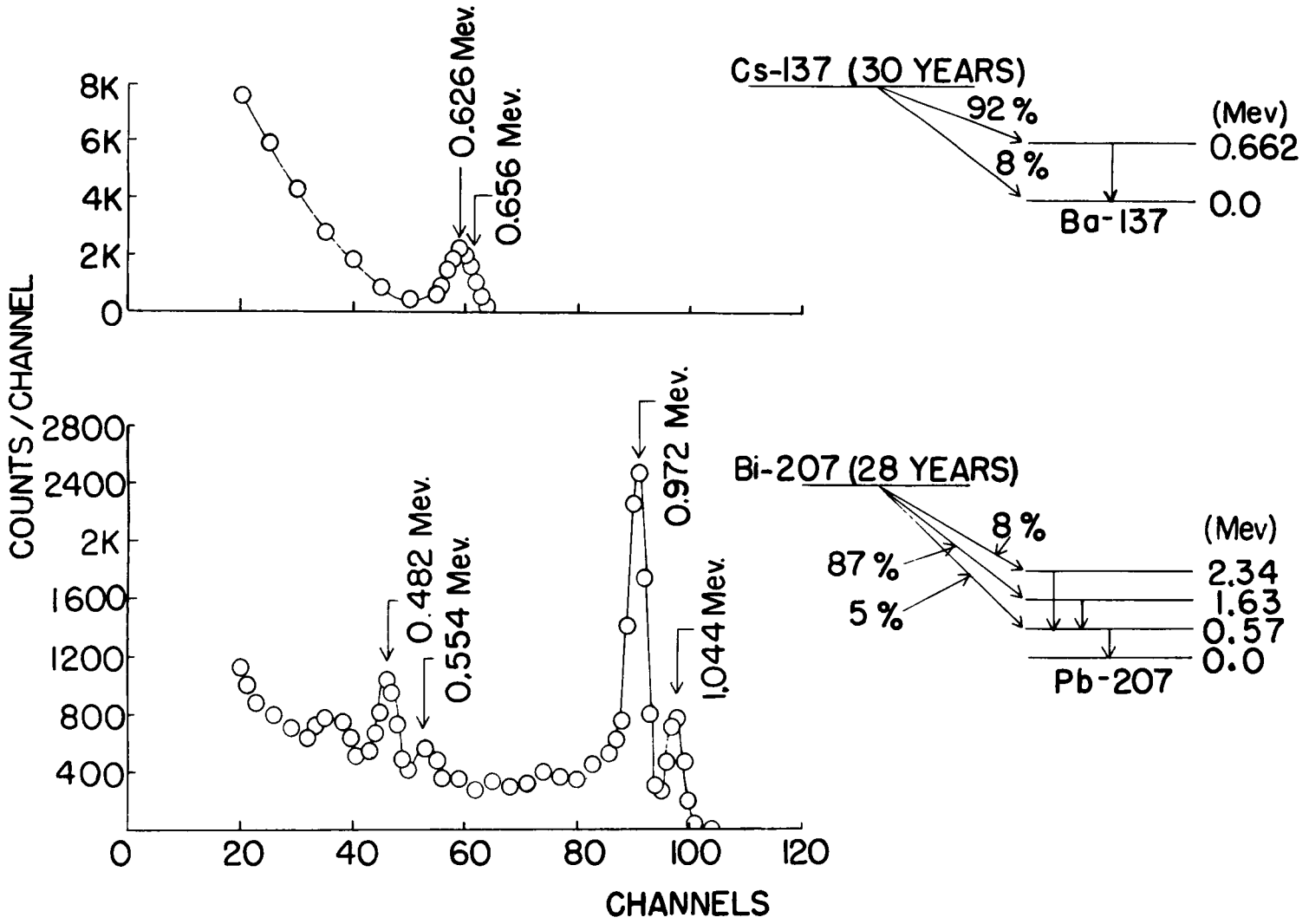

Figure 2.- Calibration spectra (Cs^{137} and Bi^{207}).

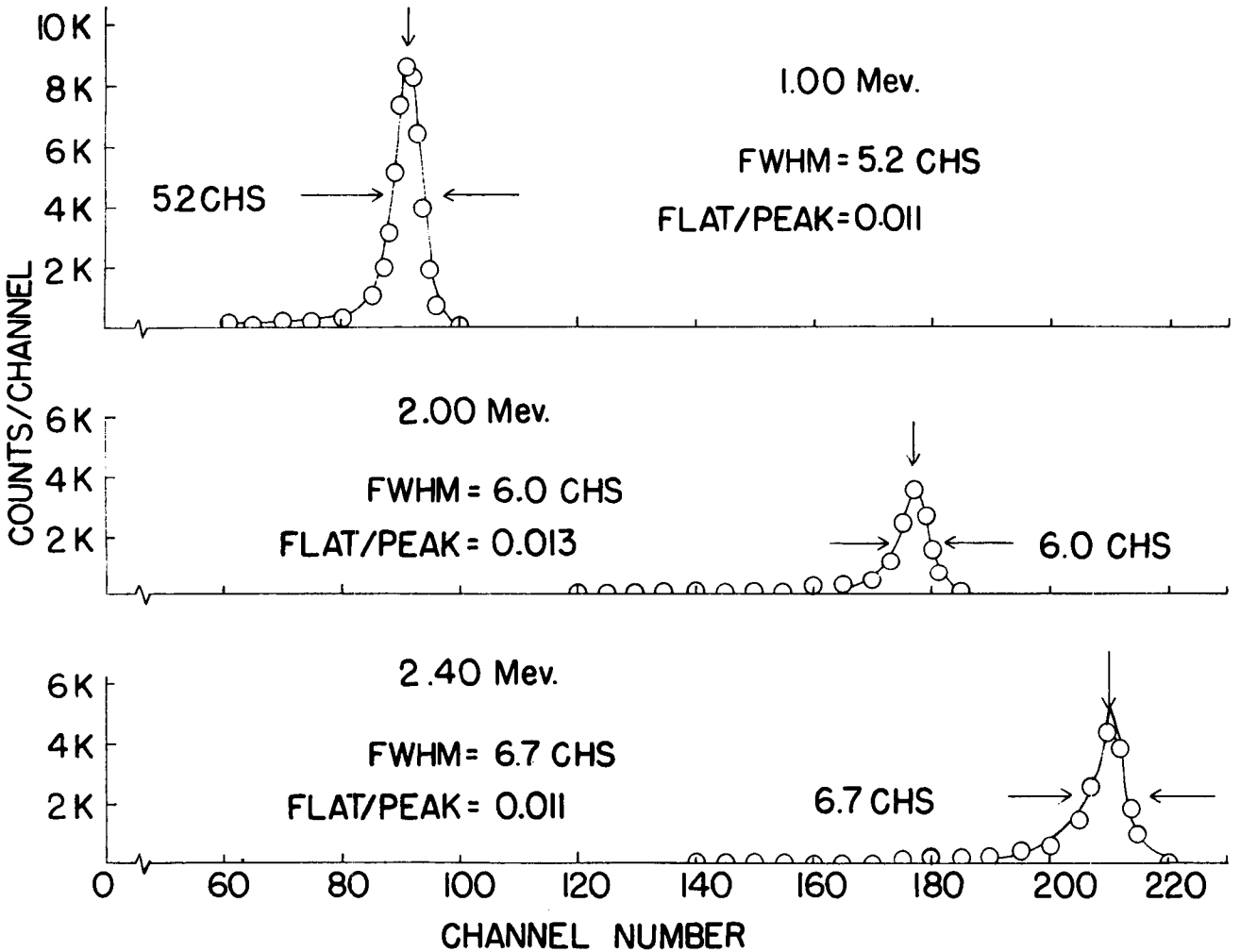

Figure 3.- Spectra of mono-energetic electrons scattered from thin $(100\mu GM/CM^2)$ gold targets.

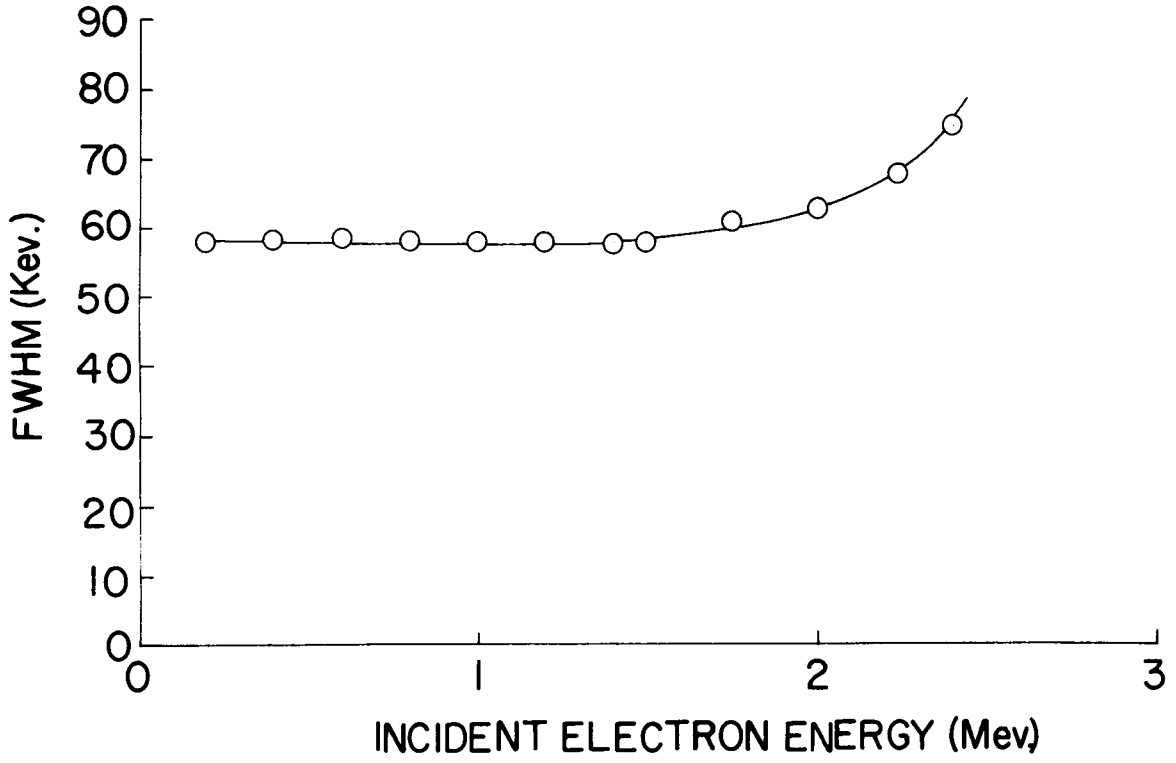

Figure 4.- Dependence of the resolving power of the detection system on the electron energy.

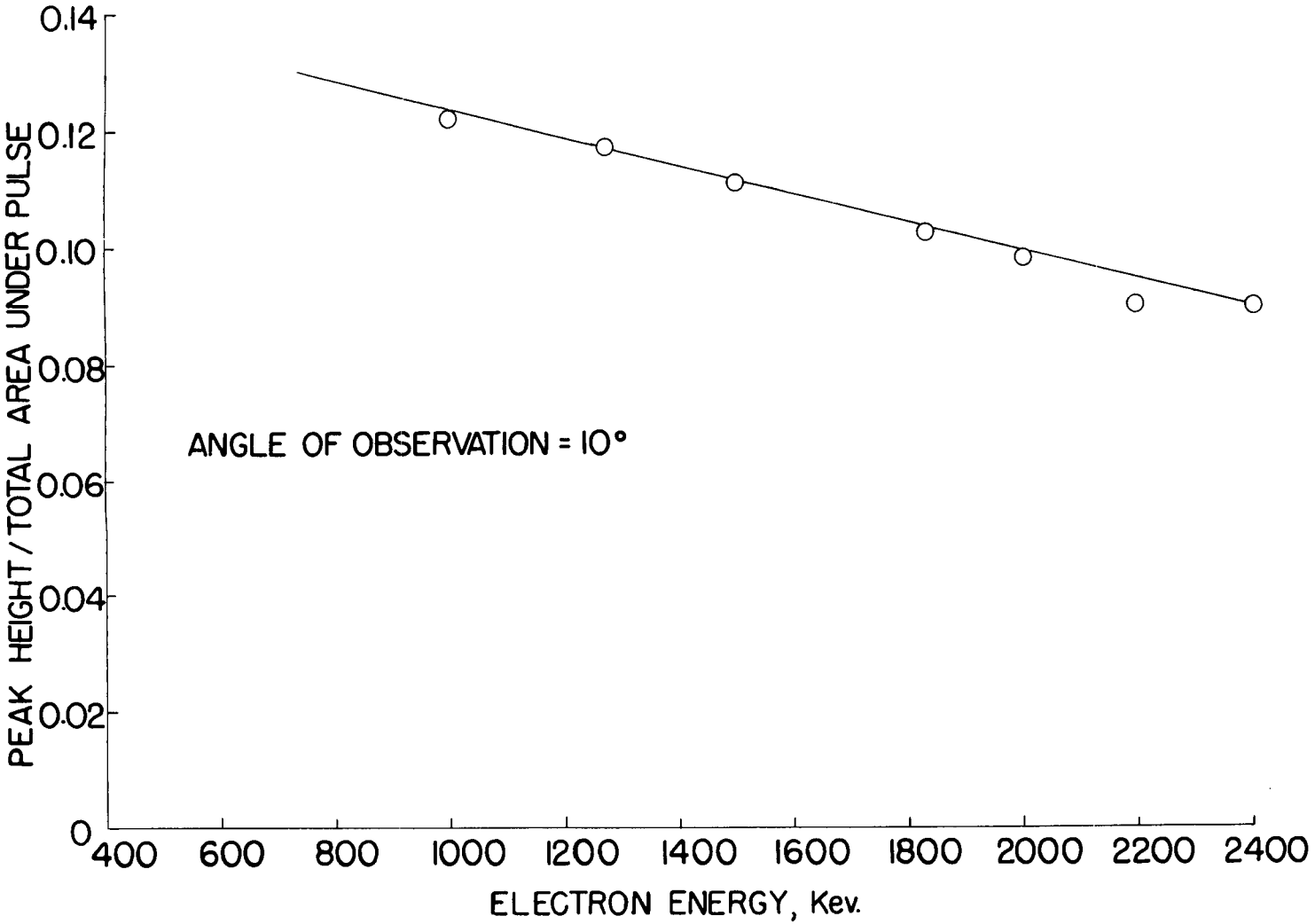

Figure 5.- Dependence of(peak height/total area under pulse) on the electron energy.

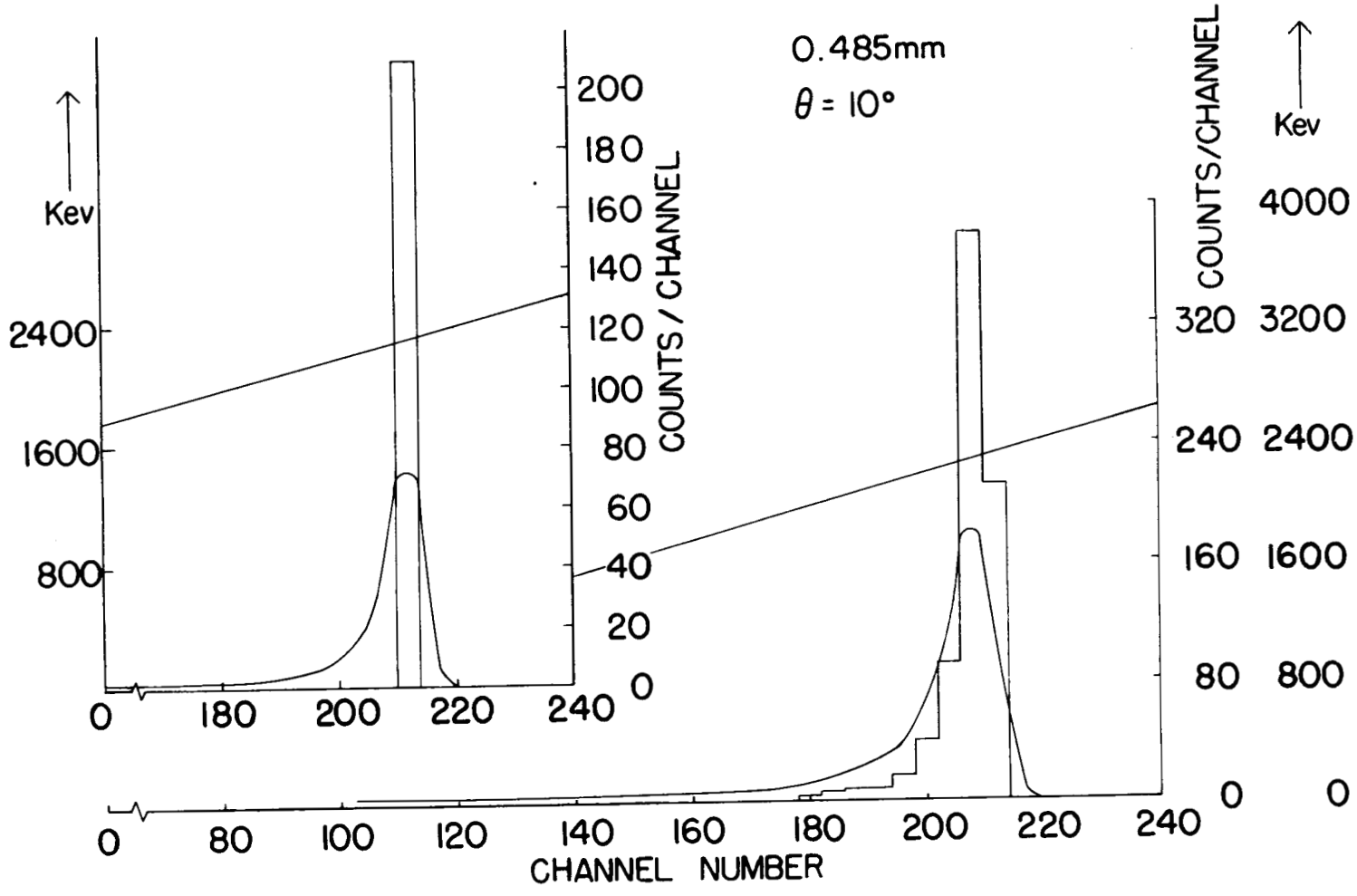

Figure 6.- Technique of modifying the theoretical histogram for the effects of finite resolution of the detection system.

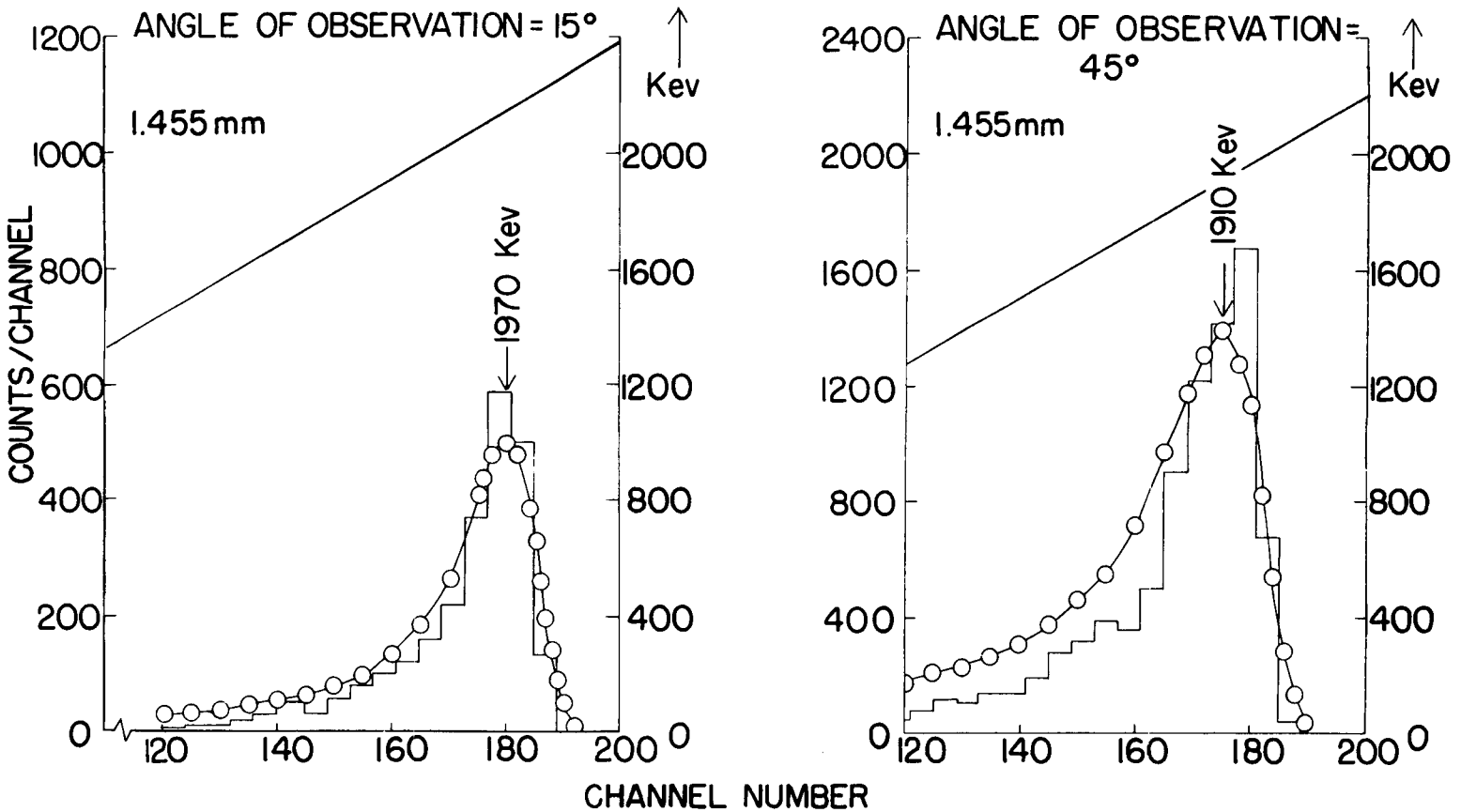

Figure 7.- Comparison of the theoretical energy histogram and the experimental energy spectrum.

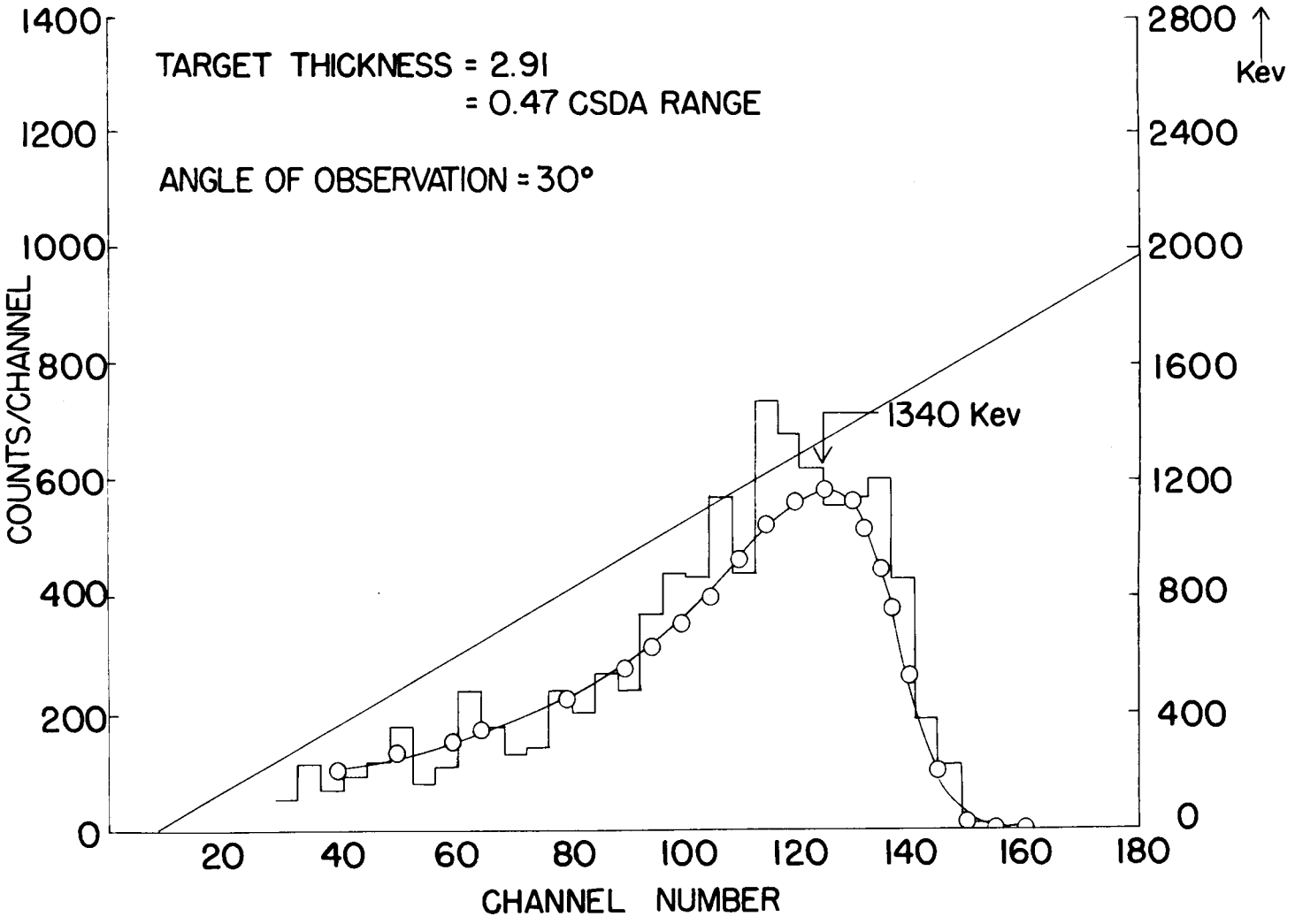

Figure 7.- Continued.

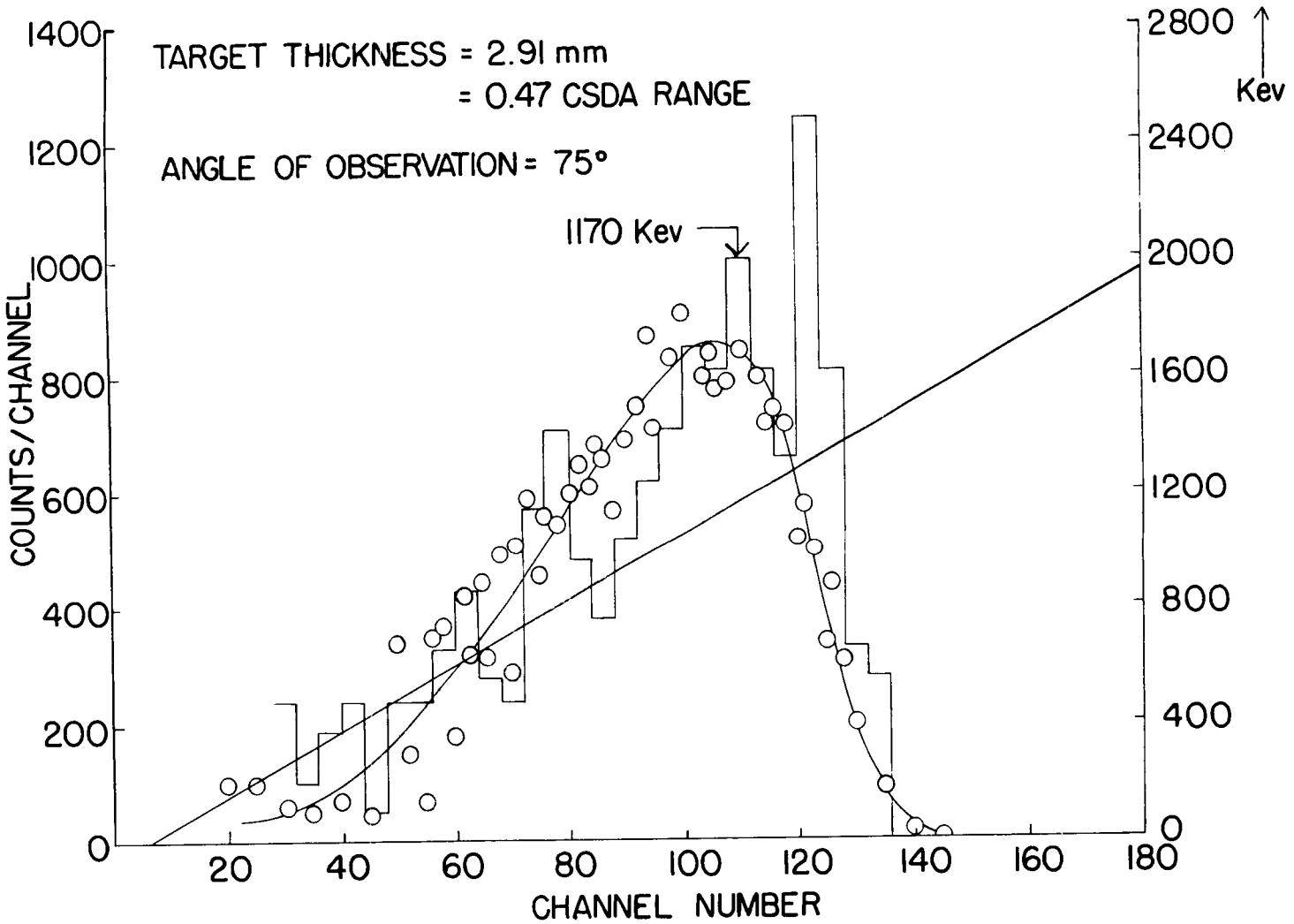

Figure 7 - Continued.

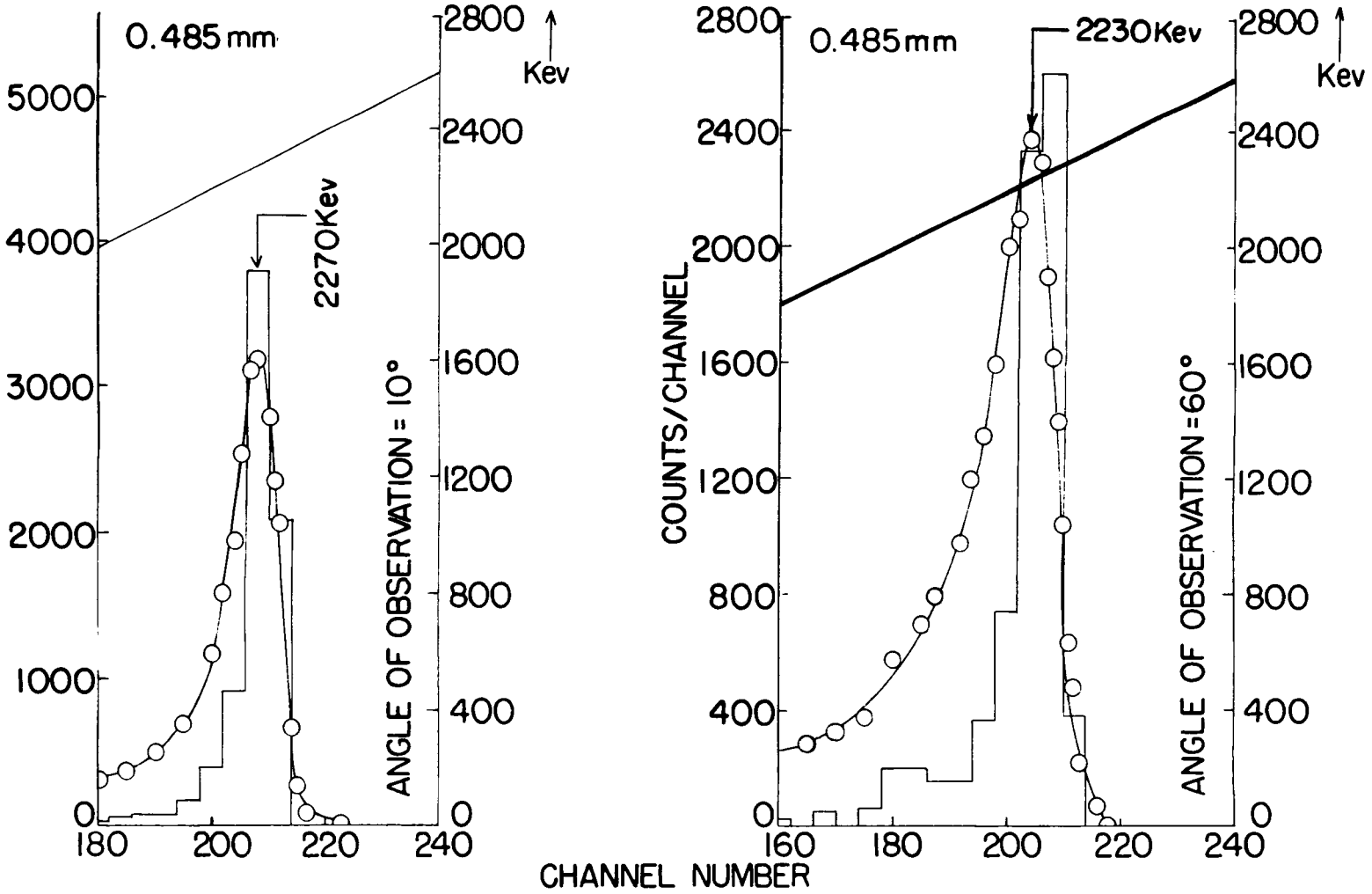

Figure 7 - Concluded.

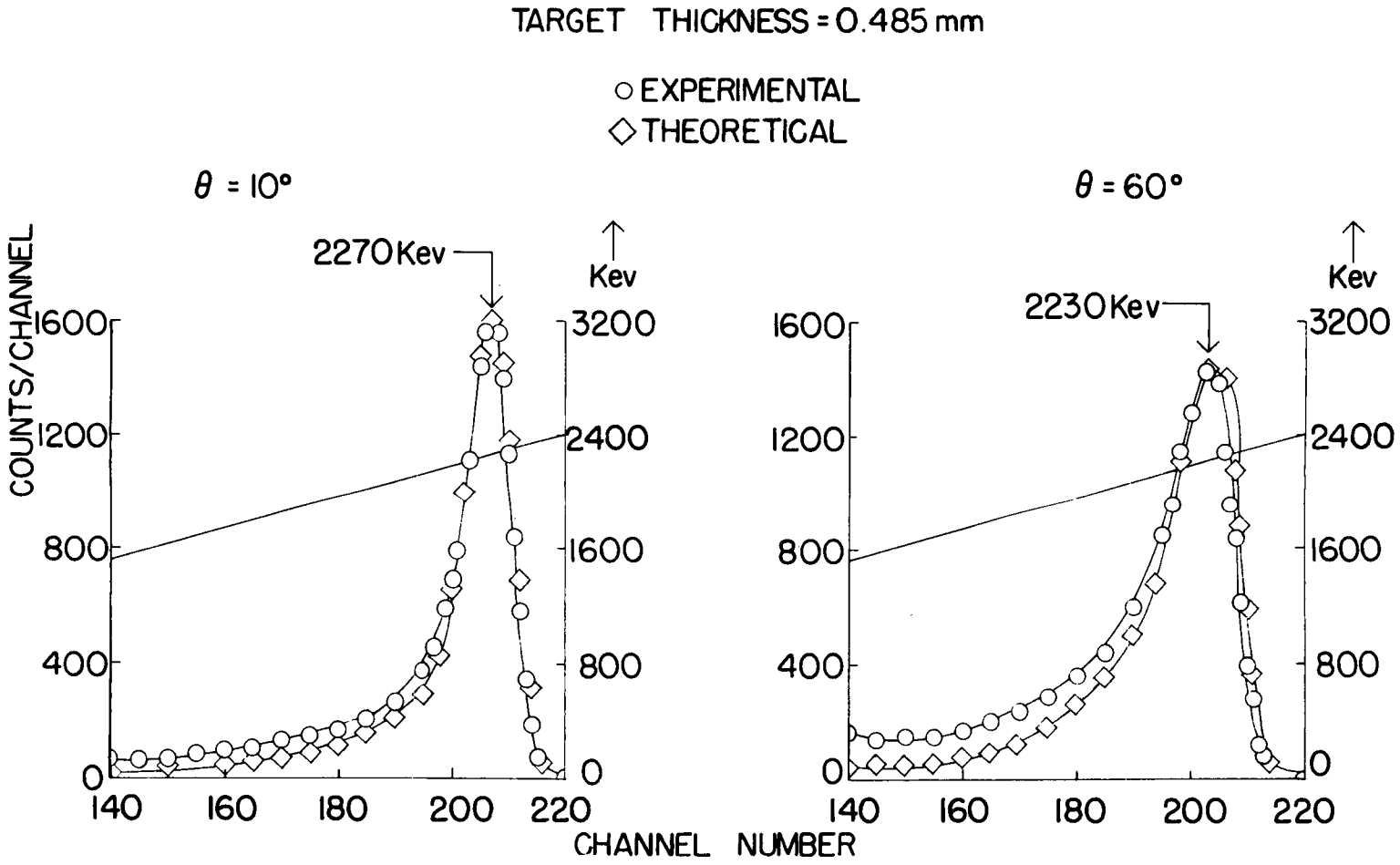

Figure 8.- Comparison of theoretical spectrum with the experimental data.

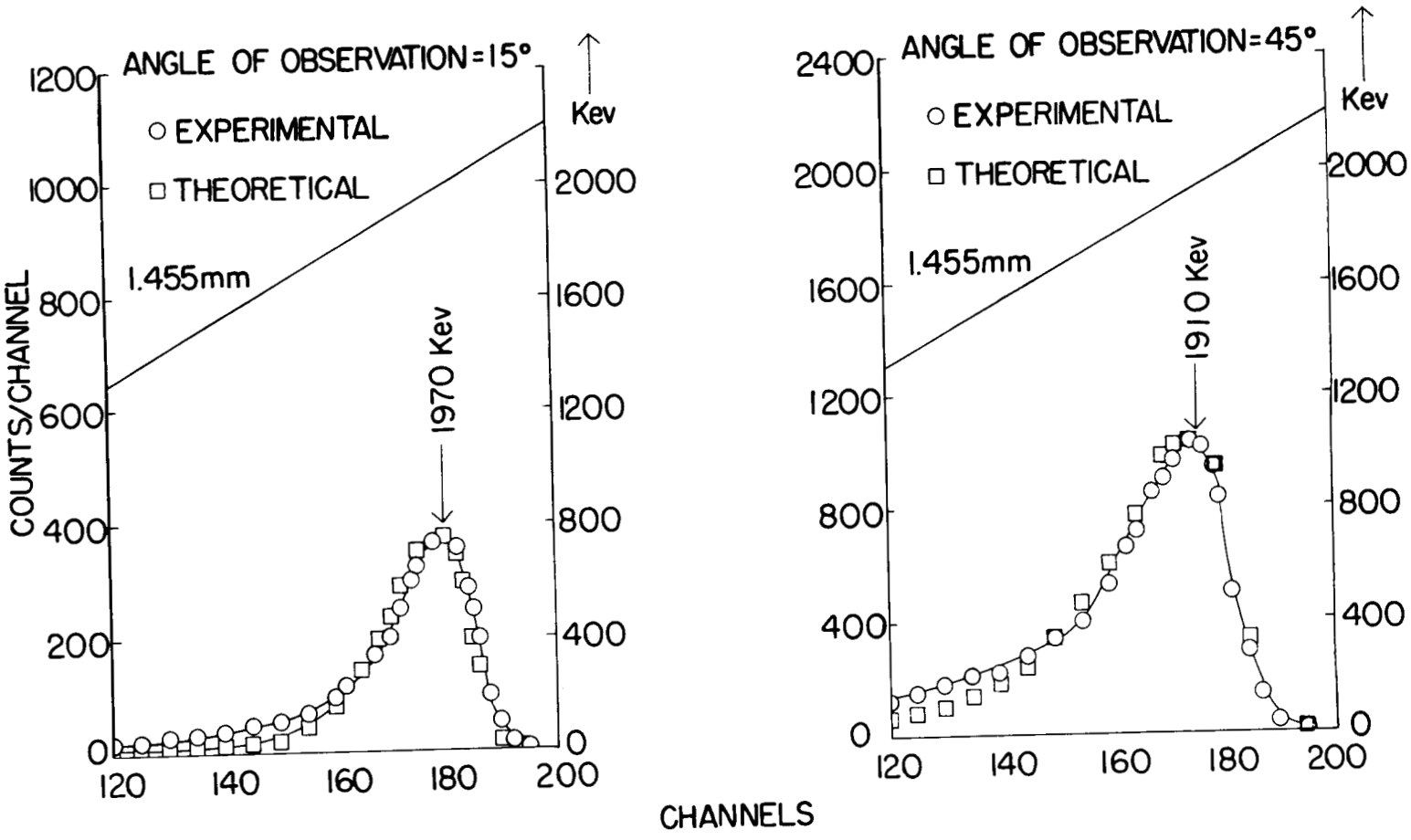

Figure 8.- Concluded.

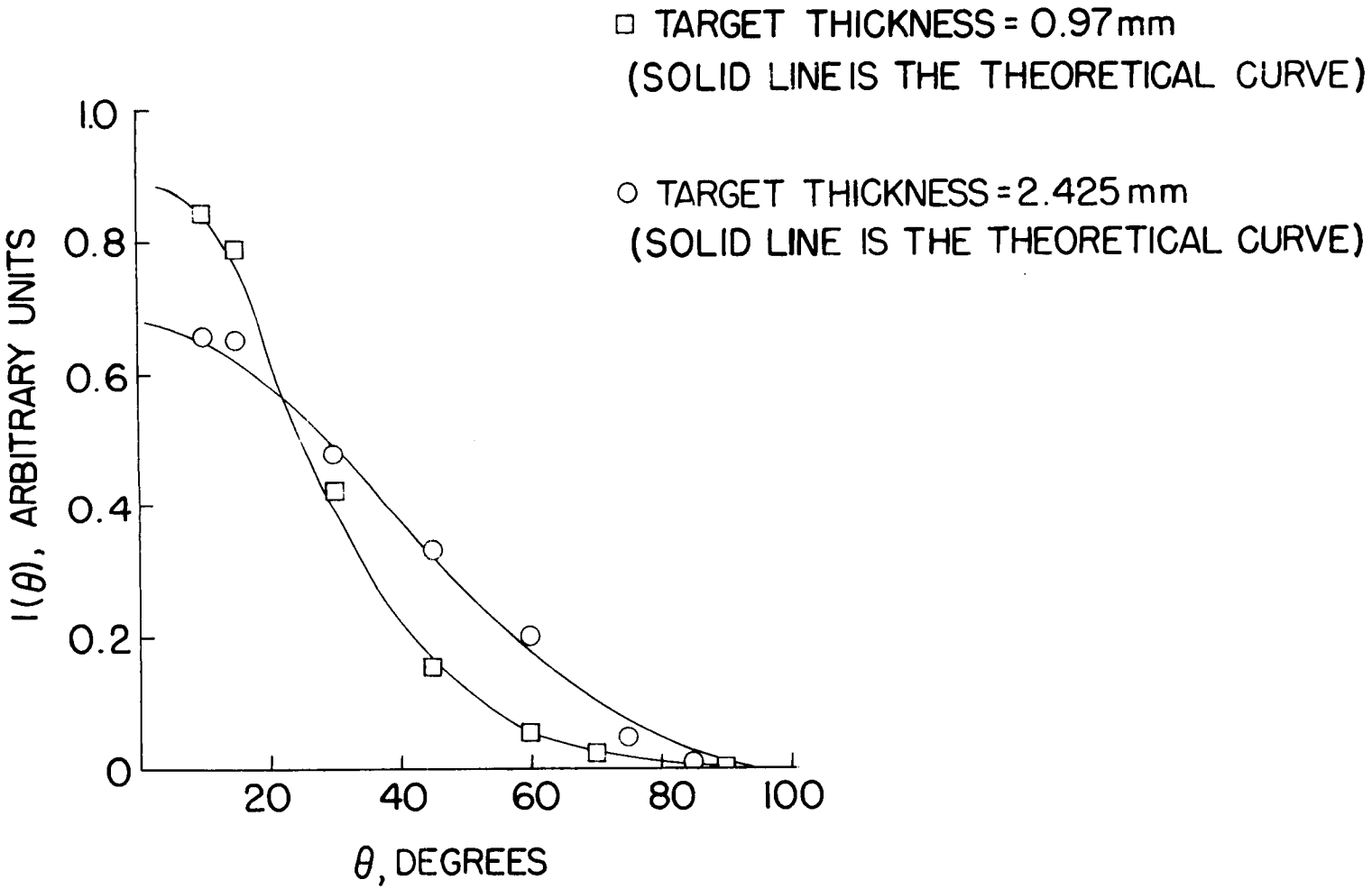

Figure 9.- Comparison of the theoretical angular distribution with the experimental distribution.

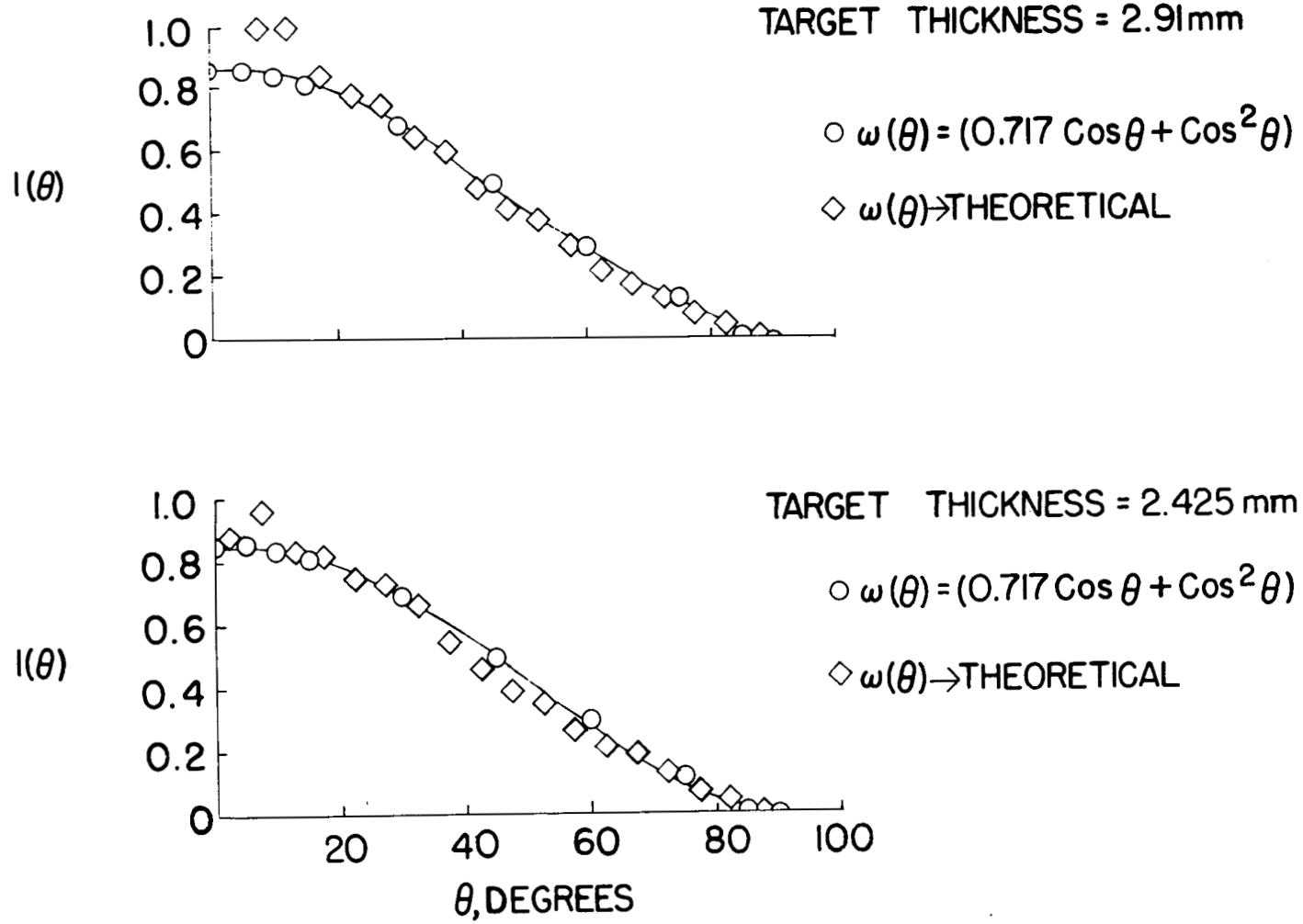

Figure 10.- Comparison of the $\frac{\text{theoretical}}{\text{Experimental}}$ angular distribution with the Bethe function.

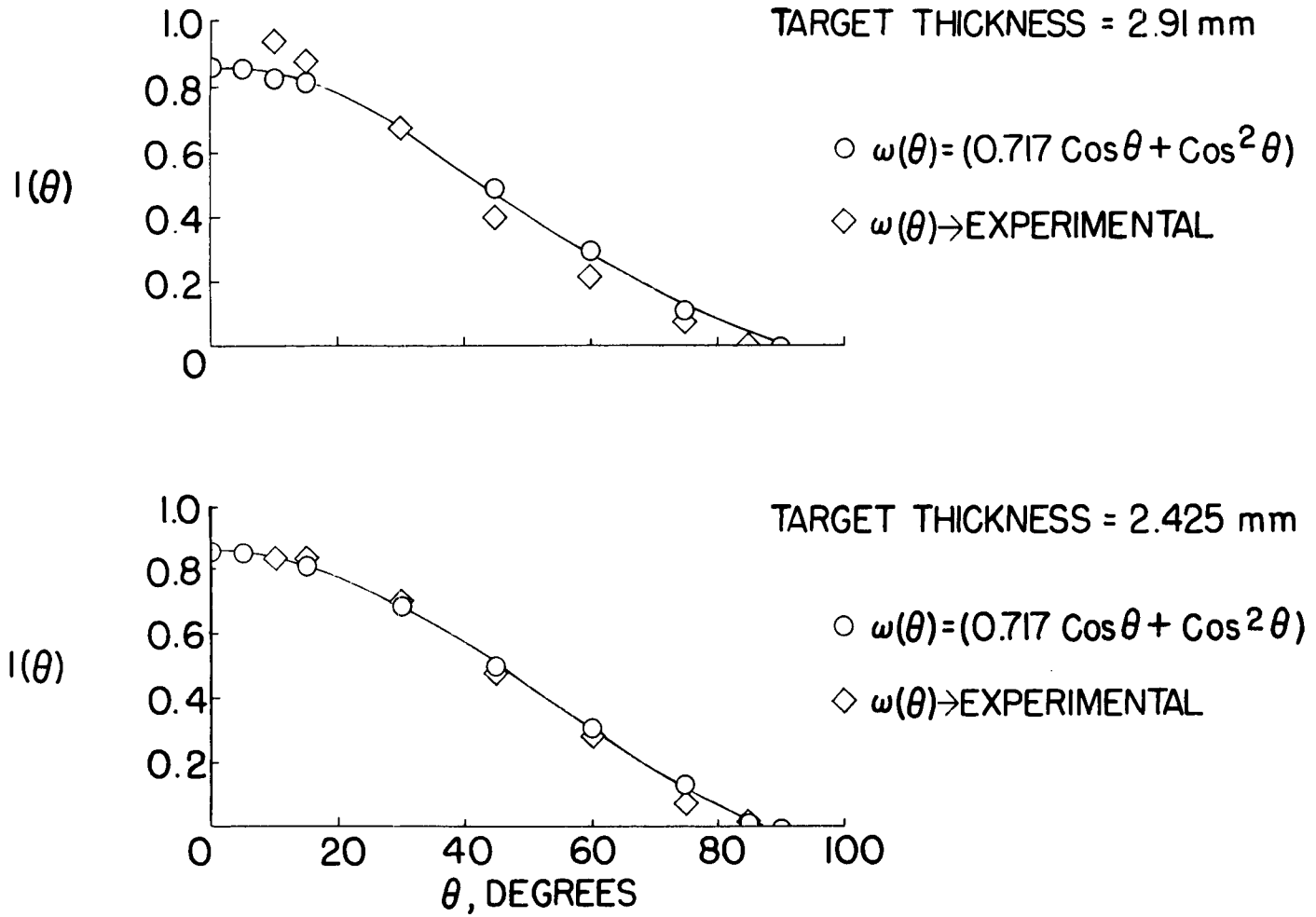

Figure 10.- Concluded.

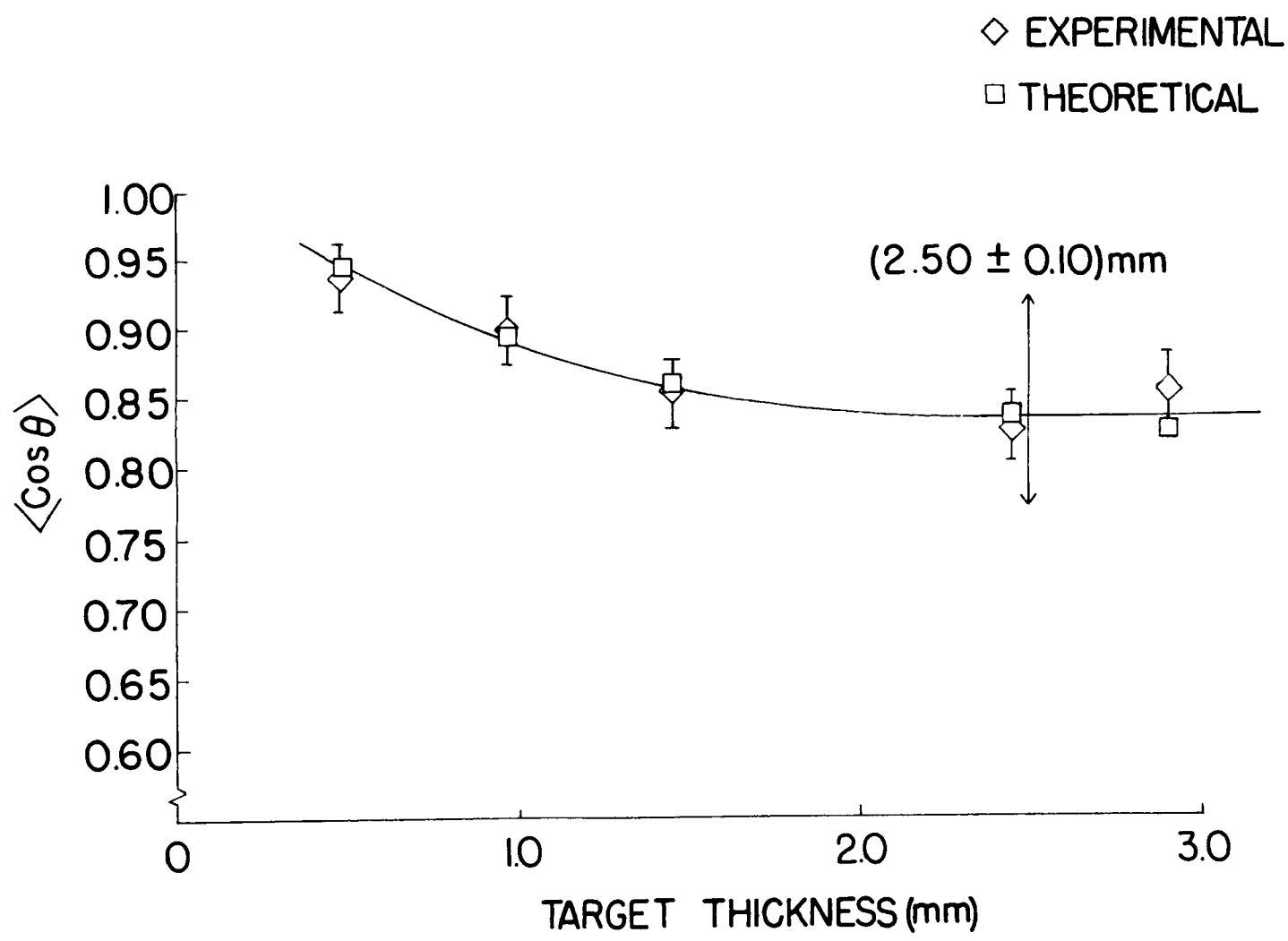

Figure 11.- <cos θ> versus target thickness.